Laser Induced Incandescence (LII) of soot †

Giorgio Zizak

CNR- TeMPE, Istituto per la Tecnologia dei Materiali e dei Processi Energetici
Via Cozzi, 53, 20125 Milano, Italy

† Lecture given at the ICS Training Course on Laser Diagnostics of Combustion Processes, NILES, University of Cairo, Egypt, 18-22 Nov. 2000

Introductory Remarks

The understanding of the processes of soot formation, and therefore the strategies for its reduction , especially in practical systems, strongly depends upon the capabilities of real-time monitoring of the soot distribution inside the flames. For such a purpose the experimental method should give a straightforward information about the amount of soot (soot volume fraction) and its location during the combustion processes. A two-dimensional temporally-resolved (or at least "single-shot") imaging technique would largely match such requirements.

Several optical techniques have been devised and applied in for soot diagnostic. *In situ* measurements of particle number density and size distribution of soot are performed with the "classical" extinction and scattering techniques. A review is presented in (Charalampopoulos, 1992). These techniques give single-point measurements and can not be practically used for the study of turbulent combustion. Two-dimensional visualization of the resonant light scattered from soot particles has been also proposed to study the structure of a sooty turbulent flame (Dasch *et alii*, 1991). Because the resonant scattering signal is proportional to the sixth power of the particle diameter, the images are strongly biased toward large particles and can not be used for soot volume fraction determination. Moreover in closed volume combustion systems the resonant signal can be seriously affected by scattering from walls and windows. Two-dimensional imaging of soot in laminar axial-symmetric flames has also been performed with 2-D extinction imaging technique followed by a tomographic deconvolution (Greenberg *et alii*, 1997, and Snelling *et alii*, 1999).

Following the pioneering works of Eckbreth (1977), Melton (1984) and Dasch (1984), recently many papers appeared in literature showing the great potentialities of the Laser-Induced Incandescence (LII) technique for 2-D visualization of soot. Although the basic principles of this technique are well understood, several uncertainties still remain for a complete theoretical description of the method. In spite of that, good quantitative measurements have been performed in a variety of experimental conditions.

In this lecture the basic theory of the LII technique will be given and several experimental considerations will be pointed out. Finally some examples of practical applications will be described.

Soot Morphology

The morphology of soot has been revealed by electron micrographs of thermophoretic sampled materials (Dobbins 1987). Soot is mainly composed by spherical particles (called primary particles) that, in a certain position of the flame, present almost the same diameter in the range 10-40 nm. These particles rapidly agglomerate in structures that, depending on the position in the flame, can be composed by a few up to thousands primary particles (figure 1). The fractal dimension of these aggregates is less than two, indicating that primary particles are not too densely packed and multiple scattering can be neglected. These observations lead to two simplifications. First, the aggregates are idealized as composed by particles of identical diameter, d_p , touching at one point. The soot volume fraction in the measurement volume is simply given by the expression:

$$f_v = (\pi/6)\, N\, n_p\, d_p^3 \qquad (1)$$

where N is the number density of aggregates and n_p is the average number of primary particles per aggregate. The second simplification assumes that the LII signal is based on the energy and mass balance between a single soot particle and its surrounding rather than the aggregate. Each particle is

independent with negligible heat transfer between primary particles. The LII signal is simply the integral over all the particles within the probe volume. A further simplification requires that temperature gradients inside the particles must be neglected.

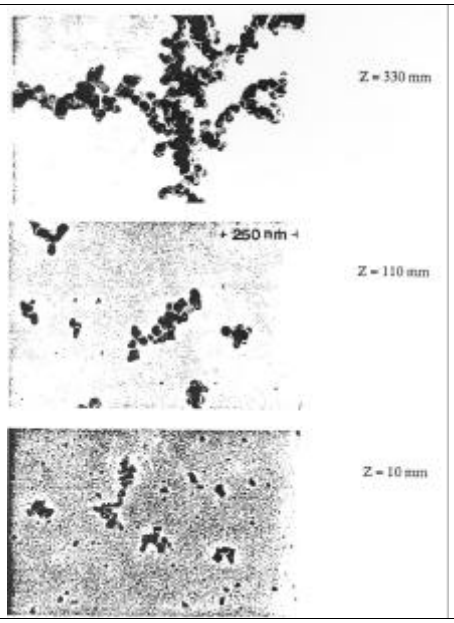

Figure 1. Soot sampled at several heights in a ethene diffusion flame (from Dobbins and Subramaniasivam, 1992)

Theoretical Considerations

The LII equations. The LII technique is based on the fact that soot particles absorb the laser light and reach, during the laser pulse, a temperature well above the flame temperature. As a consequence they emit a black body radiation that can be easily detected. With the assumptions previously described, a simple model able to describe several physical phenomena involved in the experiment was earlier developed (Eckbreth 1977, Melton 1984, Dasch 1984). In the original paper of Melton (Melton, 1984) the model the energy balance for a spherical particle of radius a, yields the following equation:

$$K_{abs}\,\pi\,a^2\,q(t) - 4\pi\,a^2\,(T-T_0)\,\Lambda - (\Delta H_v/W_s)\,dM/dt - q_{rad} - 4/3\,\pi\,a^3\,\rho_s\,C_s\,dT/dt = 0$$

where the five terms represent in the order: the absorption rate of laser energy, the rate of heat transfer to the bath gases by conduction, the energy expended in vaporization of soot carbon, the rate of energy loss by blackbody radiation and the rate of internal energy raise (figure 2). Basically, given a temporal profile of the laser pulse, q(t), the time variation of the particle radius, a, and the temperature, T, can be computed. For a correct interpretation of the signals the different terms must be carefully modeled.

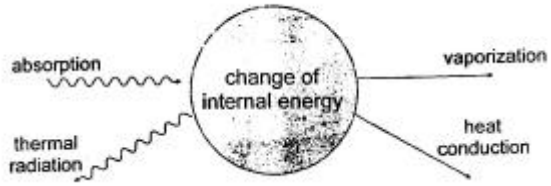

Figure 2. Schematic representation of the power balance of a laser heated soot particle (from Will *et alii*, 1998)

The absorption coefficient K_{abs} of soot depends on the absorption wavelength, λ, on the particle diameter, 2a, and on the complex index of refraction of soot, m = n+ik, and is the subject of many scientific investigations. In the Rayleigh regime ($2\pi a / \lambda << 1$) it is normally written as:

$$K_{abs} = 8 \pi a E(m) / \lambda$$

where

$$E(m) = 6 nk / [(n^2 - k^2 + 2)^2 + 4 n^2 k^2]$$

Using the relationship of Dalzell and Sarofim ((1969) we obtain at 532 nm, m = 1.59+0.58 i and $E(m)$ = 0.264, at 1064 nm m = 1.63+0.7i and $E(m)$ = 0.303.

The conductivity toward the surrounding gases, Λ, must be obtained considering that the size of primary particles is on the order of or smaller than the mean free path in the surrounding gases. Therefore it must be obtained considering both free molecule and continuum transfer regimes.

$$\Lambda = K_a / [a (1+G K_n)]$$

where K_a is the thermal conductivity in the gas, K_n is the Knudsen number (the ratio of the mean free path, l, and diameter of the particle, $K_n = l /2a$) and G is a geometric factor ($G = 8f / \alpha(\gamma+1)$, where f is the Euken factor, f = 5/2 for monoatomic species, α is an accomodation coefficient, generally adopted α = 0.9, and γ is the ratio of specific heats, assumed as for air, γ = 1.4)

The energy expended in vaporization of carbon is written in terms of heat of vaporization of carbon, ΔH_v , molecular weight of solid carbon, W_s = 12 g/mol and rate of mass vaporization, dM/dt. The vaporization model is developed from the continuity equation of the particle mass by assuming with Eckbreth (1977) that the vapor velocity is given by the thermal velocity $U_v := (RT / 2 W_v)^{1/2}$

$$dM/dt = 4\pi a^2 \rho_s da/dt = 4\pi a^2 \rho_v U_v$$

where W_v is the molecular weight of carbon vapor, taken as 36 g/mol and ρ_v is the density of carbon vapor $\rho_v = P W_v /RT$. The vapor pressure of carbon vapor is obtained by the Clapeyron formula:

$$P(T) = P^* \exp [\Delta H_v (T-T^*) /R T T^*]$$

T* is the temperature (K) at which carbon vapor pressure P equals P* (for P* = 1 atm, T* = 3915 K).

The radiative transfer q_{rad} is simply given by the Stefan-Boltzmann law for a black body:

$$Q_{rad} = 4\pi a^2 \varepsilon \sigma (T^4 - T_0^4)$$

Where σ is the Stefan Boltzmann constant and ε is the soot emissivity that can be taken equal to the absorption coefficient K_{abs}. The internal energy rise can be calculated by putting the specific heat of carbon as $C_s = 1.9$ [J/gK] and the soot density $\rho_s = 2.2$ [g/cm^3].

The above equations are coupled and must be numerically integrated in order to obtain the time dependant particle size, a(t) and temperature, T(t), for a particular choice of the excitation wavelength, λ_{exc} , flame temperature T_0 and initial particle diameter, a_0.

Finally the LII signal must be calculated taking into consideration the density of primary particles, $N_p = N\, n_p$, and the spectral bandwidth of detection, $\Delta\lambda$, around a central wavelength λ_0

$$LII(\lambda_0, t) = C1/\lambda_0^5 [\exp(-C2/\lambda_0 T(t) - 1]^{-1} N_p\, 4\pi a^2(t)\, \varepsilon(t)\, \Delta\lambda$$

Where C1 and C2 are the first and second Planck constant. By integrating the above equations Melton (Melton, 1977) showed that the LII signal at the maximum temperature (dT/dt), also called "prompt LII", is proportional to:

$$\text{prompt LII} \propto N_p\, d_p^{\,x}$$

Where d_p is the particle diameter and the exponent x is

$$x = 3 + 154\ \text{nm}/\lambda_{det}$$

For a detection wavelength, λ_{det} , in the VIS this exponent is about 3 and the prompt LII signal is proportional to the soot volume fraction. This simple finding and the easiness of the experimental set-up promoted the development of the LII technique as the major diagnostic tool for soot detection in practical combustion systems

Features of the LII signals. Several authors have investigated the features of the LII signals by developing numerical codes. The published results, obtained with slightly different codes and for different initial conditions, are not, obviously, coincident. Nevertheless, although the absolute values are different, the general features agree and well describe the experimental findings.

Figure 3 shows the calculated temperature decay for different diameters of the soot particles and for a medium peak laser power of 10^7 W/cm^2. It is possible to notice that the excess temperature and, therefore the LII signal, last for hundreds of nanoseconds. This feature is in contrast with most of the laser techniques, in which the signals are practically superimposed to the laser pulses. Moreover the peak temperature is just at the beginning of the pulse and is almost independent on the particle diameter. Finally the decay curves depend on the particle diameter with smaller particles cooling faster.

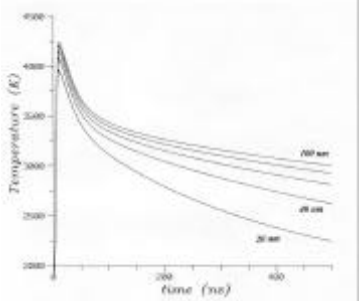

Figure 3. Calculated temperature decay for different soot diameters (10^7 W/cm^2)

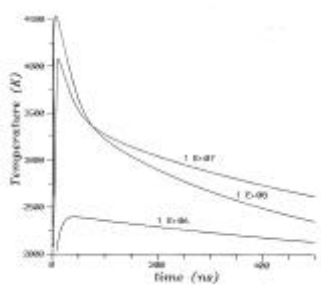

Figure 4 Calculated temperature decay for different laser power (soot diameter 40 nm)

Figure 4 reports the temperature decay curves for a particle of 40 nm in diameter and different laser powers. For low laser power density (10^6 W/cm^2) a simple heating of the particle appears, while for medium power the maximum particle temperature slightly exceeds the vaporization temperature and slowly drops down. For a very high peak power (10^8 W/cm^2) the maximum temperature reaches 4500 K and then decays faster than for a lower peak power. This is indicative of a strong vaporization process with a significant reduction in the particle mass. The relative importance of the energy loss mechanisms is shown in figure 5. It can be seen that the vaporization is the dominant mechanism for some 100 ns and that afterward the conduction term determines the temperature decay. The contribution of radiative heat transfer is small at all times.

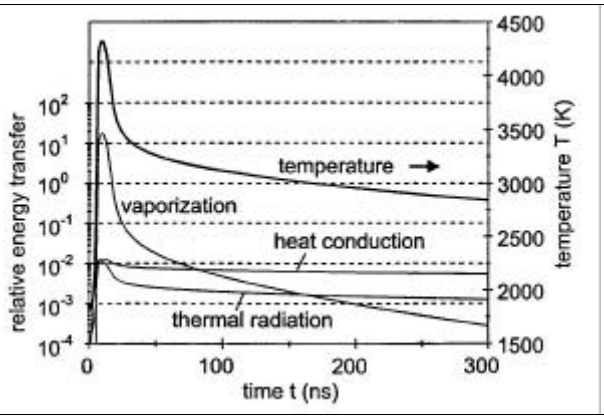

Figure 5. Comparison of the relative magnitudes of various heat loss mechanisms (from Will *et alii*, 1998).

From the temperature profiles and with the formula given above, it is possible to calculate the temporal profile of the LII signal. This is done in fig. 6 for single soot particles of different diameter. The ordinate scale is logarithmic due to the quadratic dependence of the soot incandescence signal on the particle diameter.

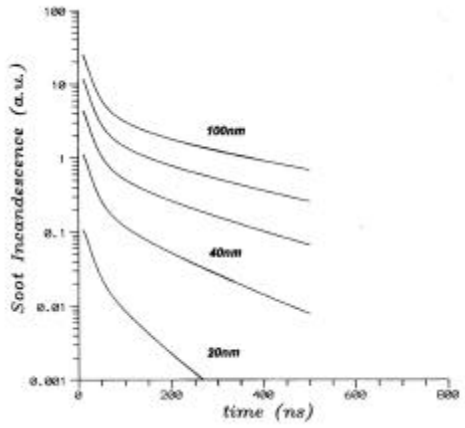

Figure 6. Calculated decay of the LII signal for different particle diameters.

The actual measured signals can be different depending on the temporal shape of the laser pulse, the energy distribution within the probe volume and the time resolution and spectral bandwidth of the measuring detector. Examples will be given in the following paragraphs.

Experimental Studies

Temporal decay of the LII signal. Many studies have been performed in the attempt to experimentally verify the general features of the LII theory. As an example figure 7 reports oscilloscope traces of the signal as measured with a PMT in two experimental conditions: a non sooty zone in a methane diffusion flames and in the soot region of a butane diffusion flame. It is evident the long decay time of the LII signal that is detectable up to 700 ns from the laser pulse.

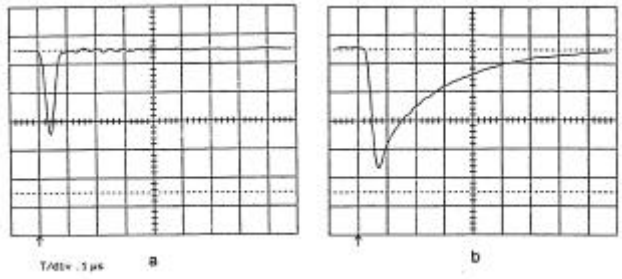

Figure 7. PMT oscilloscope traces from: (a) non sooty zone of a methane flame, (b) soot incandescence in a butane diffusion flame

From signals similar to the one in fig.7b, it is possible to draw LII signal decay curves in several regions of sooty flames. Figure 8 shows some examples obtained from measurements taken at two different heights in methane and butane diffusion flames. The decay times observed in the methane flame do not change significantly, indicating that the particle size is almost constant in the regions investigated. On the contrary strong particles growth and agglomeration is present in the butane flame. By relying on the theoretical curves, as shown in figure 6, it is possible to assume particle sizes around 25 nm for the methane flame and spanning the range 25 – 70 nm for the butane flame.

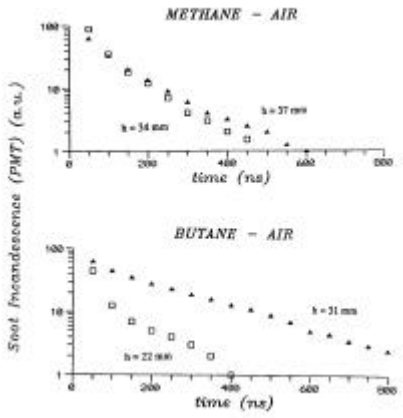

Figure 8. LII decay curves at two heights in the methane and butane diffusion flames.

In general the experimental studies reported in literature involved different excitation wavelengths, (in general obtained by a pulsed Nd.YAG laser: the fundamental at 1064, and harmonics at 532, 355 and 266 nm) different gate widths, delay times and spectral bandwidths for signal detection. The LII spectra and decay curves have been measured and compared with theoretical calculations. From the measurements soot volume fraction, particle size and temperature have been determined in a variety of sooty flames. The results confirmed the theoretical trends but many contradictions and uncertainties were evident (Quay *et alii*, 1994, Vander Wal *et alii*, 1994, Appel *et alii*, 1996, Mewes *et alii*, 1997, Schraml *et alii*, 2000). It is impossible to briefly summarize all of these studies. In this lecture it is sufficient to describe some studies concerning the dependence of the LII signal on the laser power.

LII signal versus laser fluence. As previously pointed out an important aspect of the LII technique is its the weak dependence on laser energy, once the threshold level has been reached. For nanosecond laser pulses, soot particles sizes in the range 10 – 200 nm, and temporal detection gates longer than the laser pulse duration, the key quantity which determines the dependence on power is the integrated laser intensity over the duration of the pulse (Shaddix *et alii*, 1996). This quantity is called laser fluence (J/cm^2). In fact energy conduction within the soot particle is over one order of magnitude faster than the laser pulse duration and, once the soot particle is heated to its vaporization temperature, the losses during the laser pulse are dominated by vaporization. Therefore the energy loss is sensitive to the total energy absorbed rather than to the peak particle temperature. Several studies have been performed on the dependence of the LII signal on the laser energy (Shaddix *et alii*, 1996, Bengtsson *et alii*, 1995, Ni *et alii*, 1995, Quay *et alii*, 1994). Figure 9 shows some experimental points and the predicted LII signal versus the laser fluence for a 100 nm particle for two energy distributions of the laser beam in the probe volume, a “top heat” distribution (rectangular beam) and a Gaussian beam profile. In all cases there is an initial sharp increase in the LII signal followed by a flattening. This behavior is due to two competing effects: an increase of the laser fluence makes both the peak LII signal and a the decay rate (due to soot particles loosing significant mass) to increase. Increased peak intensity leads to increased signal whereas an increase in decay rate leads to a reduction in the integrated signal over the detector gate width. This effect becomes dominant at very high fluences and, for a rectangular profile, leading to a reduction in the LII signal. In contrast, for a Gaussian profile, the signal is almost flat at very high fluences. This

behavior is explained by the increase of the number of particles above the incandescence threshold and, therefore, by the enlargement of the probe volume (wing effect).

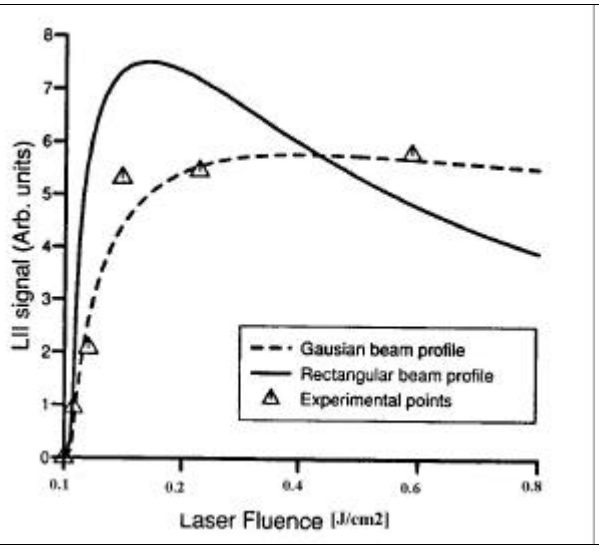

Figure 9. Predicted LII signal versus laser fluence for 100 nm particle (adapted from Tait *et alii*, 1993).

This simple picture of the physical effects involved in the LII signal is in part modified and/or contradicted by recent studies of Vander Wall (Vander Wal *et alii*, 1995, Vander Wal *et alii*, 1998). In these studies laser irradiated soot material has been sampled and analyzed by electron microscopy technique (TEM) showing substantial morphological changes.

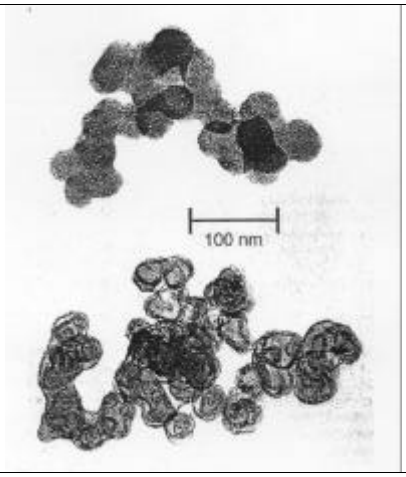

Figure 10. TEM images of typical flame soot (top) and of soot heated by the laser (bottom)(from Vander Wal *et alii*, 1998).

Figure 10 shows an image of typical soot aggregates thermophoretically captured in the flame without (top) and with (bottom) the laser passing through the flame. The size of the particles appear to be almost the same but, in contrast to the non-irradiated particles, the primary particles composing the laser-heated aggregate exhibit a noticeable structure. Banded ribbons composed by groups of parallel lines appear both within the primary particles and along the perimeter. These bands are comprised by stacks of carbon-atom layer planes. The relative transparency of the central region of the primary particles, relative to the non-irradiated soot, is due to a central void within the primary particles structure. By analogy with heat treatment studies on carbon black, it appears that the soot structure acquires considerable fluidity at elevated temperatures, allowing thermal annealing to occur. The formation of graphitic shells can naturally occur during the cooling process of the laser heated soot. Because graphite possesses a higher density than amorphous carbon, the graphitic shells have a higher density than the original carbonaceous soot. Formation of a graphitic shell without a change in particle diameter suggests a mass rearrangement with the formation of a central void. Only at very high laser fluences a loss of mass due to vaporization is involved in the LII process.

These three mechanisms, heating, graphitization and vaporization of soot can explain the simultaneous pulsed laser transmission and LII experiment. Figure 11 shows the relations between (a) the transmitted laser energy and (b) the LII signal with incident laser fluence in a premixed sooting flame. Three regimes are evident. Up to about 0.2 J/cm^2 soot is heated with a linear absorption of the laser energy and a steep and steady increase of the LII signal. In the region 0.2 – 0.4 J/cm^2 the graphitization process takes place with an incandescence signal independent on the laser fluence in spite of the linear increase in energy absorption. For fluences higher than 0.5 J/cm^2 the reduction of the LII signal is due to soot vaporization shown by the increase in laser energy transmitted through the flame.

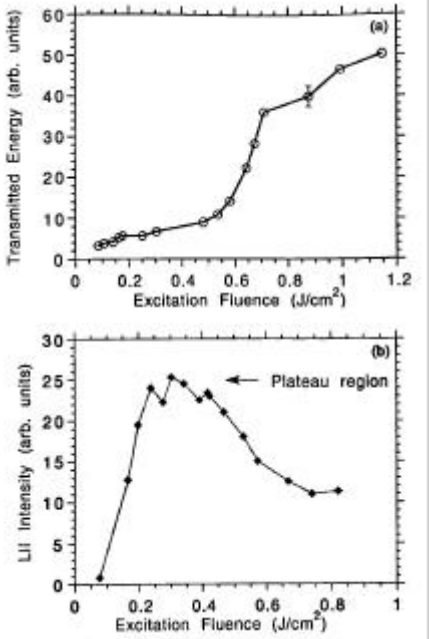

Figure 11. (a) Pulsed energy transmitted through the flame. (b) LII signal variation with incident laser fluence (from Vander Wal *et alii*, 1998)

Soot Volume Fraction Measurements

In spite of the difficulties in describing all the physical aspects involved in the LII processes, many researches have reported good agreement between soot volume fraction measurements as obtained with the LII method and with other independent diagnostic techniques. Moreover the easiness in obtaining a two-dimensional visualization of the soot distribution prompted the application of the 2D LII technique for the study of many turbulent sooty flames. In this paragraph some examples of soot volume fraction measurements and visualizations will be given.

2D imaging of soot volume fraction and validation in laminar flames. Figure 12 shows a typical and simple experimental arrangement for 2D imaging of soot distribution. The green (532 nm) beam of a pulsed Nd.YAG laser is vertically expanded through a cylindrical lens and focussed in the horizontal direction by a spherical lens on the axis of the flame. The light sheet is about 30 cm in height with a thickness of about 350 μ. An aperture limits the height of the sheet to about 10 cm to ensure uniformity of the laser sheet. Typical pulse energy is in the order of 300 mJ/pulse.

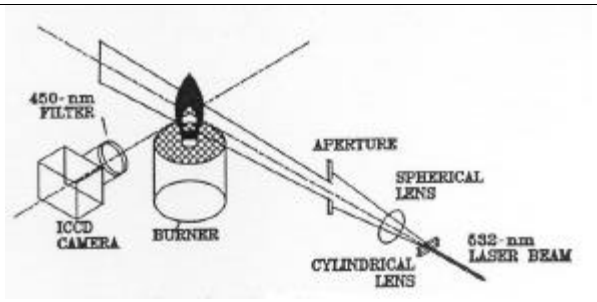

Figure 12. Typical experimental set-up for 2D LII imaging (from Ni *et alii*, 1995)

The LII images are taken at 90° angle by a gatable intensified CCD camera equipped with a camera lens. A broadband filter in the blue (450 ± 25 nm) is placed in front of the camera to minimize the interference from scattered light. Depending on the experimental situation a complete reduction of the scattered light is performed by gating the camera just after the laser pulse. A gate width of about 20 ns for the intensifier is used to minimize the effect of particle size. Possible interferences from PAH fluorescence are minimized by gate delay (Cignoli *et alii*, 1994), and by antiStokes detection (long wavelength excitation and short wavelength detection). The LII images are then calibrated on a single point and compared with soot profiles obtained with the laser extinction technique (Abel inversion of a lateral extinction profile and application of the "classical" formula for the determination of radial soot volume fraction profile). Some results obtained with this procedure are shown in figure 13. Two diffusion flames are investigated, a methane and an ethylene axialsymmetric flame. LII and extinction profiles are reported for several heights in the flame. The arrow in the methane flame, at 40 mm height, indicates the calibration point. Excellent agreement is evident in the methane flame. The somewhat wider profiles exhibited by the extinction data likely arise from the signal averaging required by these measurements. Reasonable agreement is also found for the ethylene flame. The agreement is excellent toward the centerline, with appreciable differences in the annular soot layer. These differences can be ascribed to slightly different flame conditions during the two experiments. Based on these measurements, the uncertainty in the LII calibration relative to the extinction-derived soot measurements is approximately ± 10 % over soot volume fraction ranging from 0.05 to 10 ppm (a factor of 200), effective soot particle sizes from 300 to 115 nm (i.e. volume-equivalent spheres), and number densities from $2\ 10^9$ to $2\ 10^{10}$ cm^{-3} (assuming a monodisperse size distribution).

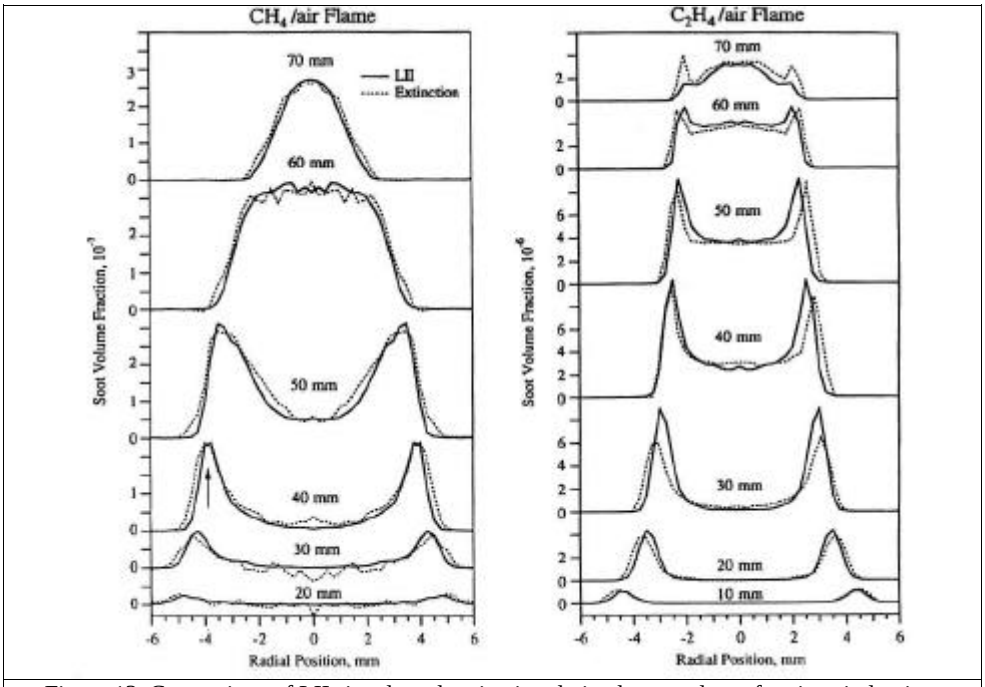

Figure 13. Comparison of LII signals and extinction derived soot volume fractions in laminar diffusion flames. The LII measurements are calibrated to the peak soot volume fraction in the 40 mm height of the methane flame (arrow) (from Shaddix *et alii*, 1996).

The calibration procedure based on the extinction is rather cumbersome and prone to significant uncertainties, mainly due to weak signal in small laminar flames and to the poorly known refractive index of soot. Other calibration procedures have been attempted by employing a gravimetric sampling technique (Vander Wal *et alii*, 1996) and a Cavity Ring-Down technique (Vander Wal, 1998).

2-D visualization of soot in a diesel engine. The first application of the LII technique for practical studies was done by Dec (Dec *et alii* , 1991, Dec, 1992) for the investigation of the formation of soot in a diesel engine. Figure 14 shows a schematic of the experimental arrangement. The engine was a modified single cylinder direct-injection diesel engine. The light sheet was obtained by the frequency doubled pulsed Nd:YAG laser with a power level of 1.6 10^8 W/cm^2. The spray axis was 18° downward from horizontal and the visibility of the soot distribution, obtained by the laser sheet, was limited by the optical thickness of the spray plume. Suitable filters were used to suppress the background luminosity and elastic scattering. Figure 15 gives an example of a temporal sequence of LII images taken in the plane 11.1 mm below the cylinder head for a low-sooting (top) and reference (bottom) fuels. The most striking feature of the top images is that soot is present through the center of the spray as well as the edges of the imaged cross section. These data suggest that combustion over the sooting portion of the plume may be a more volumetric process than implied by the term “diffusion” burn commonly used in the diesel engine literature. The bottom images, relative to the reference fuel, show a soot distribution along the periphery of the plume. This is interpreted by considering the optical thickness of the reference fuel, not allowing the laser sheet to cut a section through the plume.

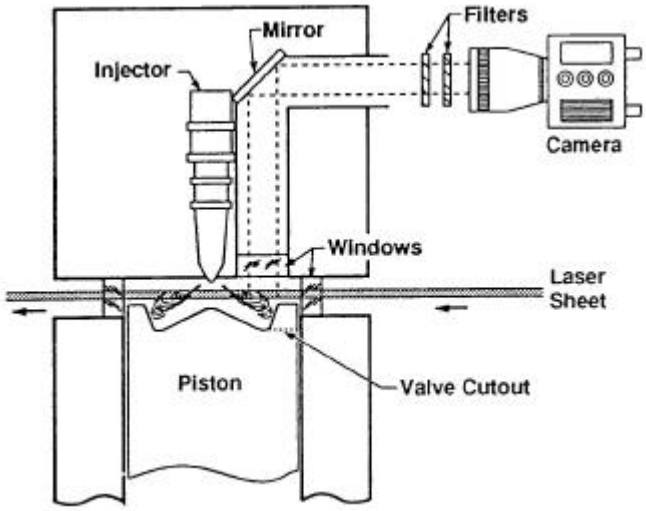

Figure 14. Schematic of the engine and optical configuration (from Dec *et alii* 1991).

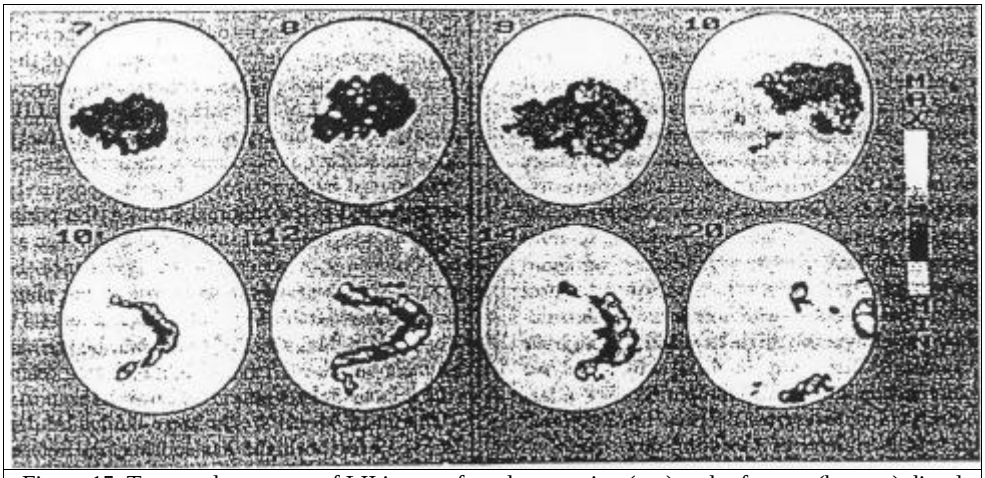

Figure 15. Temporal sequence of LII images for a low-sooting (top) and reference (bottom) diesel fuel (from Dec *et alii*, 1991).

Simultaneous visualization of multiple species in gas-jet diffusion flames. Taking advantage of the spectral coincidence in the absorption band of different species, it is possible to visualize two or more species simultaneously (Cignoli *et alii*, 1992). Polycyclic aromatic hydrocarbons (PAH's) are considered precursors of soot. These molecules present absorption bands in the UV and a red-shifted emission in the UV-VIS part of the spectrum. By the use of the fourth harmonic of a pulsed Nd:YAG laser, soot LII and PAH's laser induced fluorescence can be simultaneously visualized. This has been demonstrated by Vander Wal (Vander Wal *et alii*, 1997).

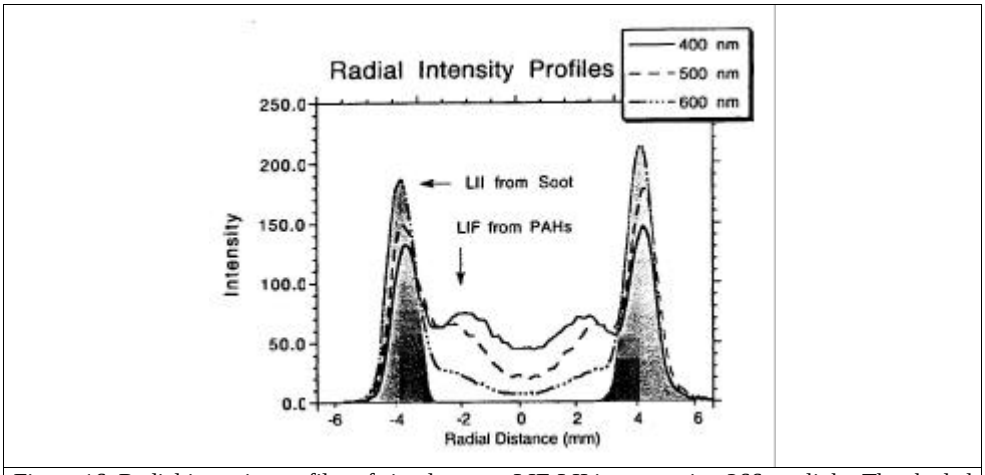

Figure 16. Radial intensity profiles of simultaneous LIF-LII images using 266 nm light. The shaded region denotes the annular soot containing region. (from Vander Wal *et alii*, 1997).

Figure 16 shows the radial intensity profiles obtained by using a 266 nm laser beam and different band pass interference filters. The profiles contain contributions from both soot LII signal (shaded region) as verified from LII images obtained with a 1064 nm laser beam and laser-induced fluorescence (LIF) from polycyclic aromatic hydrocarbons. Figure 17 shows a two-dimensional visualization of the diffusion flame structure.

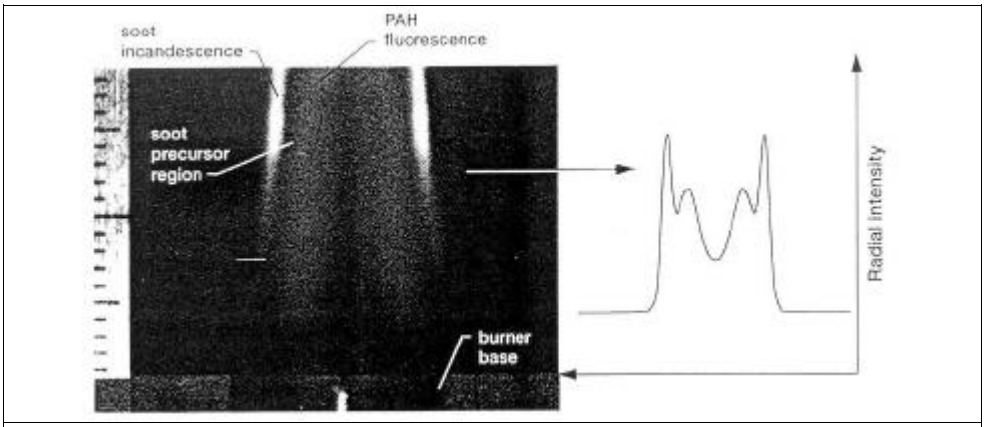

Figure 17. 2-D visualization of soot and PAH's in an ethylene diffusion flame (from Vander Wal *et alii*, 1997).

By using a pulsed XeCl excimer laser tuned at 308 nm, Tait (Tait *et alii*, 1993) studied a turbulent propane jet flame of Reynolds number ≈ 10^4. Figure 18 shows the structure of this flame.

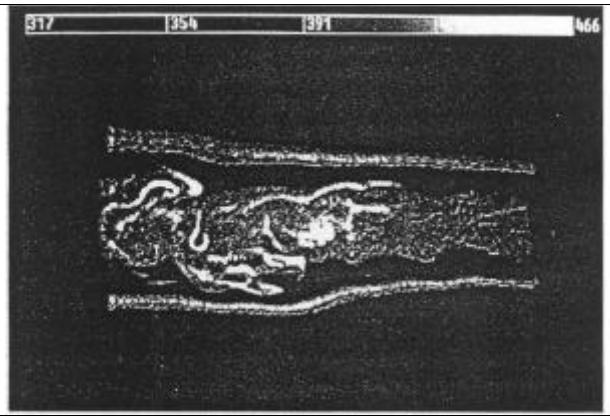

Figure 18. LIF- LII image in a propane jet flame (from Tait *et alii*, 1993).

In the flame there are contributions from OH and PAH's fluorescence as well as LII and Mie scattering from soot. The higher viscosity at the flame front re-laminarises the flow so that the OH forms a laminar sheet around the more turbulent core. The soot occurs in sheets that are formed in the fuel rich high temperature regions, near the flame front, and are then vortically mixed into the core.

Advanced Diagnostic Techniques.

As described in the previous paragraphs, the LII technique is experimentally rather simple. However, due to the peculiar characteristics of the LII signal several exploitations are possible. These have been the subject of several papers, with the development of two basic techniques.

The TIRE-LII technique. The basic idea of the time-resolved LII (TIRE-LII) technique is to measure the incandescence signal at two different times, at least, during the cooling of the soot particles and to calculate a signal ratio, which can be unambiguously connected to the size of soot particles (Will *et alii*, 1995, Will *et alii*, 1996). There are no basic theoretical constraints on the choice of the observation times, however it is suggested to avoid the first vaporization period and to allow a sufficient time span between the measurements for sufficient particle size sensitivity. A good compromise has been found to be timing the measurements at 100 ns and 800 ns after the excitation laser pulse; however for soot volume fraction, f_v , measurements a "prompt" LII signal must be measured. Therefore when a single gatable intensified CCD camera and appropriate filters are available, two dimensional images of soot volume fraction and particle size can be obtained only in stationary flames. For turbulent flames studies, two and/or three identical cameras and filters must be used for single-shot images. Figure 19 shows the results of this technique as applied to the study of a simple stationary ethene diffusion flame. The soot volume fraction distribution of the left figure was obtained by the "prompt" LII and calibration with an integral extinction signal. An annular region of maximum soot concentration and a decrease of f_v due to oxidation processes with increasing height can be observed. The TIRE-LII technique has been used for the figure on the right where the primary particle size distribution is shown. In the annular region the particles reach about 80 nm in diameter while on the axis the particle size falls in the range 20-30 nm. These values are

slightly higher then the ones reported in literature for similar flames. The lack of knowledge about the actual local gas temperature and composition can explain the considerable uncertainties present in the model employed in this study.

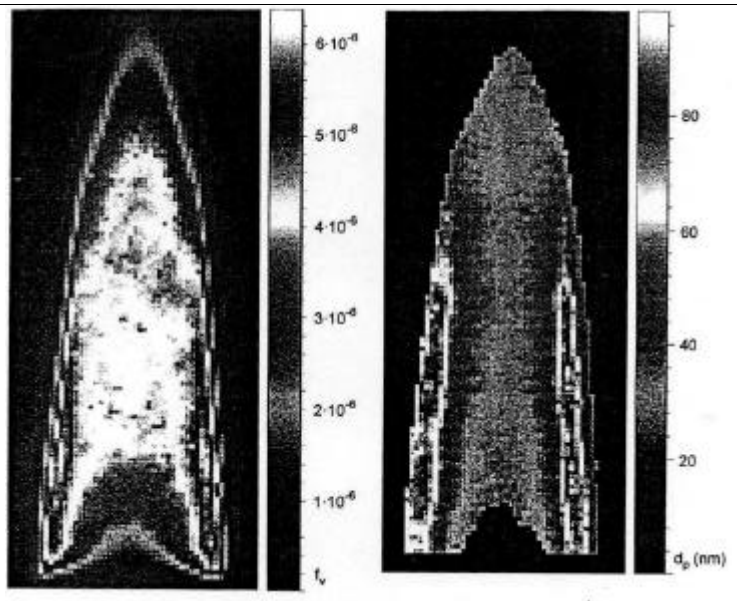

Figure 19. Soot volume fraction (left) and particle diameter (right) from prompt and TIRE-LII technique in an laminar ethene diffusion flame (from Will *et alii*, 1996).

The RAYLIX technique. The knowledge of the physical meaning of the scattered and LII signals resulted in the realization of a complex experimental apparatus for soot diagnostics in turbulent flames. The new technique is based on the two-dimensional detection of Rayleigh scattering and LII signal in combination with detection of extinction (RAYLIX) (Geitlinger *et alii*, 1998, and 1999). It is known that in the Rayleigh regime, the Rayleigh scattering is proportional to the laser intensity and to the sixth power of the particle radius. The LII signal is proportional to the third power of the radius and is almost independent on the laser power. The extinction is used to correct for laser absorption by the soot particles. All signals are detected simultaneously and extinction is used to calibrate the relative LII signal for absolute soot volume fraction. The experimental apparatus is shown in figure 20. Very briefly the central idea of the technique is to split the laser pulse into two delayed pulses with the plate G1. The first pulse of low energy, is used to obtain an image of the Rayleigh scattering from soot, avoiding any incandescence signal; the second strong pulse, delayed through mirrors S2 and S3, is used for LII imaging. Two gatable CCD cameras detect the Rayleigh and LII images in coincidence with the respective pulses. The twp plates G2 and G3 are inserted in the apparatus to obtain the images of the laser sheet intensity distributions before and after the flame. These images are realized in quartz cuvettes K1 and K2 filled with a dye solution. The images are visualized side by side of the Rayleigh image. Data processing is rather cumbersome (ratioing the images and taking into account the soot extinction) but reliable images have been obtained. Figure 21 reports the images of the volume fraction, particle number density and size in a turbulent acetylene flame.

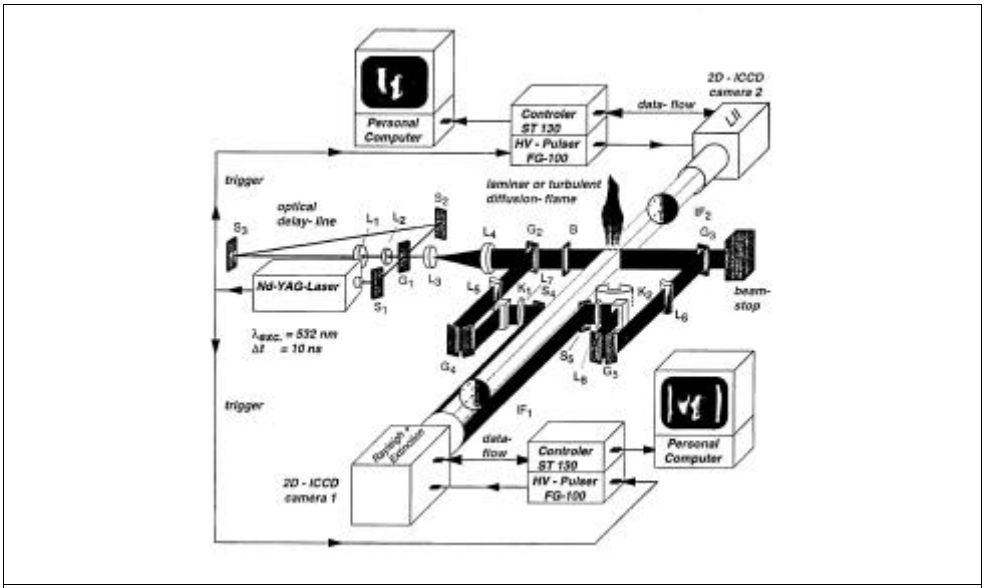

Figure 20. RAYLIX set-up for turbulent flame studies (from Geitlinger *et alii*, 1998)

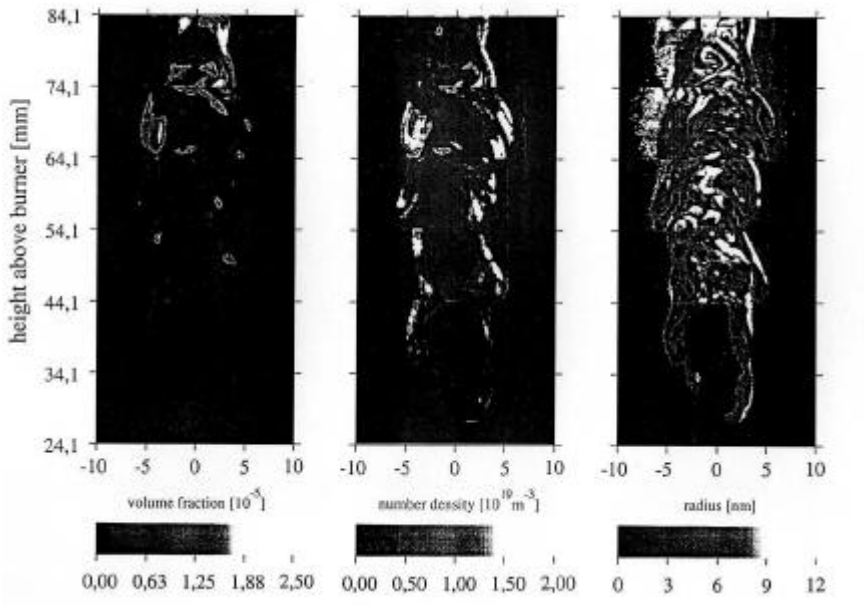

Figure 21. Two-dimensional fields of soot volume fraction, particle number density and radius in a turbulent diffusion flame (from Geitlinger *et alii*, 1998).

References

Appel, J., Jungfleisch, B., Marquardt, M., Suntz, R., Bockhorn, H., (1996); Assessment of soot volume fraction from laser-induced incandescence by comparison with extinction measurements in laminar, premixed, flat flames, *26th Symposium (Int.) on Combustion*, The Combustion Institute, 2387-2395.

Bengtsson, P.-E., Alden, M., (1995); Soot-visualization strategies using laser techniques, *Appl.Phys. B*, **60**, 51-59.

Cignoli, F., Benecchi, S., Zizak, G., (1992); Simultaneous one-dimensional visualization of OH, polycyclic aromatic hydrocarbons, and soot in a laminar diffusion flame, *Opt.Lett.*, **17**, 229-231.

Cignoli, F., Benecchi, S., Zizak, G., (1994); Time-delayed detection of laser-induced incandescence for the two-dimensional visualization of soot in flames, *Appl.Optics*, **33**, 5778-5782.

Charalampopoulos, T.T., (1992); Morphology and dynamics of agglomerated particulates in combustion systems using light scattering techniques, *Prog.Energy Combust.Sci.*, **18**, 13-45.

Dalzell, W.H., Sarofim, A.F., (1969); Optical constants of soot and their application to heat flux calculations, *J.Heat Transfer*, **91**, 100-104.

Dasch, C.J., (1984); Continuous-wave probe laser investigation of laser vaporization of small soot particles in a flame, *Applied Optics*, **23** (13), 2209-2215.

Dasch, C.J., Heffelfinger, D.M. (1991); Planar imaging of soot formation in turbulent ethylene diffusion flames: fluctuations and integral scales, *Comb.Flame*, **85**, 389-402.

Dec, J.E., zur Loye, A.O., Siebers, D.L., (1991); Soot distribution in a D.I. diesel engine using 2-D laser-induced incandescence imaging, *SAE paper 910224*.

Dec, C.J., (1992); Soot distribution in a D.I. diesel engine using 2-D imaging of laser-induced incandescence, elastic scattering, and flame luminosity, *SAE paper 920115*.

Dobbins, R.A., Megaridis, C.M., (1987); Morphology of flame-generated soot as determined by thermophoretic sampling, *Langmuir*, **3**, 254-259.

Dobbins, R.A., Subramaniasivam, H., (1992); Incipient particle formation in hydrocarbon flames, *Work-in-progress Poster presented at the 24th Symposium (Int.) on Combustion*, Sydney, Australia, 5th-10th July 1992.

Eckbreth, A.C., (1977); Effects of laser-modulated particulate incandescence on Raman scattering diagnostics, *J.Appl.Phys.*, **48** (11), 4473-4479.

Geitlinger, H., Streibel, Th., Suntz, R., Bockhorn, H., (1998); Two-dimensional imaging of soot volume fraction, particle number densities, and particle radii in laminar and turbulentdiffusion flames, *27th Symp. (Int.) on Combustion*, The Combustion Institute, 1613-1621.

Geitlinger, H., Steibel, Th, Suntz, Bockhorn, H., (1999); Statistical analysis of soot volume fractions, particle number densities and particle radii in a turbulent diffusion flame, *Comb.Sci.and Technol.*, **149**, 115-134.

Greenberg, P.S., Ku, J.C., (1997); Soot volume fraction imaging, *Applied Optics*, **36**, 5514-5522.

Melton, L.A., (1984); Soot diagnostics based on laser heating, *Applied Optics*, **23** (13), 2201-2208.

Mewes, B., Seitzman, J.M., (1997); Soot volume fraction and particle size measurements with laser-induced incandescence, *Appl.Optics*, **36**, 709-717.

Ni, T., Pinson, J.A., Gupta, S., Santoro, R.J., (1995); Two-dimensional imaging of soot volume fraction by the use of laser-induced incandescence, *Appl.Opt.*, **34**, 7083-7091.

Quay, B., Lee, T.-W., Ni, T., Santoro, R.J., (1994); Spatially resolved measurements of soot volume fraction using laser-induced incandescence, *Comb.Flame*, **97**, 384-392.

Shaddix, C.R., Smyth, K.C., (1996); Laser-induced incandescence measurements of soot production in steady and flickering methane, propane, and ethylene diffusion flames, *Comb.Flame*. **107**, 418-452.

Schraml, S., Dankers, S., Bader, K., Will, S., Leipertz, A., (2000); Soot temperature measurements and implications for time-resolved laser-induced incandescence (TIRE-LII), *Comb.Flame*, **120**, 439-450.

Snelling, D.R., Thomson, K.A., Smallwood, G.J., Gulder, O.L., (1999); Two-dimensional imaging of soot volume fraction in laminar diffusion flames, *Applied Optics*, **38**, 2478-2485.

Tait, N.P., Greenhalgh, D.A., (1993); PLIF imaging of fuel fraction in practical devices and LII imaging of soot, *Ber.Bunsenges.Phys.Chem.*, **97**, 1619-1624.

Vander Wal, R.L., Weiland, K.J., (1994); Laser-induced incandescence: development and characterization towards a measurement of soot volume fraction, *Appl.Phys. B*, **59**, 445-452.

Vander Wal, R.L., Choi, M.Y., Lee, K.-O., (1995); The effects of rapid heating of soot: implications when using laser-induced incandescence for soot diagnostics, *Comb.Flame*, **102**, 200-204.

Vander Wal, R.L., Zhou, Z., Choi, M.Y., (1996); Laser-induced incandescence calibration via gravimetric sampling, *Comb.Flame*, **105**, 462-470.

Vander Wal, R.L., Jensen, K.A., Choi, M.Y., (1997); Simultaneous laser-induced emission of soot and polycyclic aromatic hydrocarbons within a gas-jet diffusion flame, *Comb.Flame*, **109**, 399-414.

Vander Wal, R.L., (1998); Calibration and comparison of laser-induced incandescence with Cavity Ring-Down, *27Th Symposium (Int.) on Combustion*, The Combustion Institute, 59-67.

Vander Wal, R.L., Jensen, K.A., (1998); Laser-induced incandescence: excitation intensity, *Appl.Optics*, **37**, 1607-1616.

Will, S., Schraml, S., Leipertz, A., (1995); Two-dimensional soot-particle sizing by time-resolved laser-induced incandescence, *Opt.Letters*, **20**, 2342-2344.

Will, S., Schraml, S., Leipertz, A., (1996); Comprehensive two-dimensional soot diagnostics based on laser-induced incandescence (LII), *26th Symp.(Int.) on Combustion*, The Combustion Institute, 2277-2284.

Will, S., Schraml, S., Bader, K., Leipertz, A., (1998); Performance characteristics of soot primary particle size measurements by time-resolved laser-induced incandescence, *Applied Optics*, **37**, 5647-5658.